APL Materials

Dislocations as channels for the fabrication of sub-surface porous GaN by electrochemical etching

Cite as: APL Mater. **8**, 031115 (2020); https://doi.org/10.1063/1.5142491
Submitted: 13 December 2019 . Accepted: 05 March 2020 . Published Online: 25 March 2020

Fabien C.-P. Massabuau, Peter H. Griffin, Helen P. Springbett, Yingjun Liu, R. Vasant Kumar, Tongtong Zhu, and Rachel A. Oliver

ARTICLES YOU MAY BE INTERESTED IN

Encapsulation of methylammonium lead bromide perovskite in nanoporous GaN
APL Materials **7**, 021107 (2019); https://doi.org/10.1063/1.5083037

Structural characterization of porous GaN distributed Bragg reflectors using x-ray diffraction
Journal of Applied Physics **126**, 213109 (2019); https://doi.org/10.1063/1.5134143

Structural and electronic properties of the pure and stable elemental 3D topological Dirac semimetal α-Sn
APL Materials **8**, 031114 (2020); https://doi.org/10.1063/1.5142841

© 2020 Author(s).

Dislocations as channels for the fabrication of sub-surface porous GaN by electrochemical etching

Cite as: APL Mater. 8, 031115 (2020); doi: 10.1063/1.5142491
Submitted: 13 December 2019 • Accepted: 5 March 2020 •
Published Online: 25 March 2020

Fabien C.-P. Massabuau, Peter H. Griffin, Helen P. Springbett, Yingjun Liu, R. Vasant Kumar, Tongtong Zhu,[a] and Rachel A. Oliver[a]

AFFILIATIONS

Department of Materials Science and Metallurgy, University of Cambridge, 27 Charles Babbage Road, Cambridge CB3 0FS, United Kingdom

[a]**Authors to whom correspondence should be addressed:** tongtong.zhu@porotech.co.uk and rao28@cam.ac.uk

ABSTRACT

Porosification of nitride semiconductors provides a new paradigm for advanced engineering of the properties of optoelectronic materials. Electrochemical etching creates porosity in doped layers while leaving undoped layers undamaged, allowing the realization of complex three-dimensional porous nanostructures, potentially offering a wide range of functionalities, such as in-distributed Bragg reflectors. Porous/non-porous multilayers can be formed by etching the whole, as-grown wafers uniformly in one simple process, without any additional processing steps. The etch penetrates from the top down through the undoped layers, leaving them almost untouched. Here, atomic-resolution electron microscopy is used to show that the etchant accesses the doped layers via nanometer-scale channels that form at dislocation cores and transport the etchant and etch products to and from the doped layer, respectively. Results on AlGaN and non-polar GaN multilayers indicate that the same mechanism is operating, suggesting that this approach may be applicable in a range of materials.

© 2020 Author(s). All article content, except where otherwise noted, is licensed under a Creative Commons Attribution (CC BY) license (http://creativecommons.org/licenses/by/4.0/). https://doi.org/10.1063/1.5142491

Gallium nitride and its alloys are enabling an ever-increasing range of applications across electronics and optoelectronics. Since the development of the first commercial nitride light emitting diodes (LEDs) in the mid-1990s, the potential applications of this family of materials have burgeoned to include laser diodes,[1] single photon sources,[2] solar cells,[3] power electronic devices,[4] and integrated photonic circuits.[5] In all of these devices, the key method by which the properties of the nitride materials have been systematically engineered is by changing their composition, principally by altering the proportion of the different group III metals (indium, gallium, aluminum, and more recently boron) forming the binary compound with nitrogen.

Recently, an alternative method of engineering the materials properties of nitride semiconductors has emerged: by introducing porosity into monolithic nitride layers, it is possible to achieve very significant changes in a wide range of properties including electrical[6] and thermal[7] conductivity, refractive index,[8] birefringence,[9] mechanical properties,[10] strain relief,[11] chemical activity,[12] and piezo-electricity.[13] Porous GaN layers are already enabling enhanced device performance in LEDs[14,15] and laser diodes (LDs)[16] and the development of novel composites of GaN with other materials.[17] The porosification of other nitride alloys has allowed the formation of novel quantum structures.[18] Introducing porosity to nitride materials provides a new degree of freedom, allowing hitherto unanticipated physical phenomena and device concepts to be explored.

Porosification of GaN can be achieved by an electrochemical etching process in which highly n-doped GaN immersed in an acid-based electrolyte is subjected to a positive anodic bias.[19] This results in oxidation of GaN by holes at the surface inversion layer, resulting in material decomposition and pore formation. This mechanism requires the n-doped GaN surface to be directly exposed to the electrolyte. However, for many potential applications of porous GaN, a multilayer of alternating porous and non-porous

materials is required. A key example here is a distributed Bragg reflector (DBR) in which the refractive index contrast between layers results in reflection at the interfaces between the layers. High reflectivity occurs when the quarter-wavelength of the light incident on the DBR matches the layer thickness. For porous nitride DBRs, this typically implies the formation of a stack of several pairs of layers, consisting of a non-porous layer and a porous layer, each a few 10s of nanometers thick.

Such a structure can be formed by growing a simple (non-porous) GaN structure, consisting of alternating layers of undoped GaN (which will remain non-porous) and highly n-doped GaN (which will be porosified). In order to access the sub-surface doped layers and achieve porosity by electrochemical etching, it is typical to first cover the GaN surface with SiO_2 and then pattern this SiO_2 by opening up windows of uncovered GaN. SiO_2 is used as an etch mask in the etching of deep trenches into GaN. This exposes the sidewalls of sub-surface, highly n-doped GaN layers. Electrochemical porosification then proceeds laterally into the masked regions. This approach has been very successful for the formation of DBRs over small regions, of lateral extent 10s–100s of micrometers.[20] For example, Huang *et al.*[21] showed lateral etching over a range of about 80 μm, and Hsu *et al.*[22] showed a greater etch penetration of 155 μm. Lateral etching has been used to create optically pumped microcavities[8] and electrically injected laser structures.[16] However, the requirement to etch deep trenches at regular intervals adds significant complexity and cost to the cheap and simple electrochemical etching process and is limiting in terms of device design.[23]

For porous GaN to be integrated into existing device processing paradigms, it would be preferable to develop a simple process that allows uniform porosification of sub-surface layers across whole industrial-size wafers, without the requirement for surface coating and trench etching. We recently demonstrated[14] such a wafer-scale porosification approach for the formation of DBRs, and the same approach is relevant to a broad range of other sub-surface multilayer structures. We showed that etching can occur *through* an undoped surface GaN layer and also through the multiple undoped layers in the DBR stack, porosifying the doped layers and leaving the undoped GaN almost unaltered. We suggested that etching was occurring via intrinsic structural defects, potentially threading dislocations, which are ubiquitously present in the heteroepitaxial nitride materials that dominate the nitride device market. Here, we address the role of threading dislocations in the electrochemical etching process and reveal the details of the porosification mechanism.

For this study, structures consisting of alternating layers of undoped GaN and doped GaN were deposited by metal-organic vapor phase epitaxy (the standard industrial technique) in a 6 × 2 in. Thomas Swan close-coupled showerhead reactor on c-plane sapphire substrates using trimethylgallium and ammonia as precursors, hydrogen as a carrier gas, and silane for n-type doping. After the growth of a 4 μm thick c-plane GaN buffer layer with a nominal dislocation density of ~3×10^8 cm^{-2}, 500 nm n-doped GaN (silicon doping concentration ~ 1×10^{18} cm^{-3}) was first grown to enable the uniform distribution of etching current across the entire area of the wafer. Thereafter, pairs of alternating highly doped n^+-GaN, with a nominal silicon doping concentration of ~1×10^{19} cm^{-3}, and undoped GaN layers, with an electron concentration of $<10^{17}$ cm^{-3}, were grown.

Porosification of the sub-surface doped GaN layers was achieved using a simple one-step electrochemical etching process, as detailed elsewhere.[14] In this process, the GaN sample is immersed in 0.25M oxalic acid with the as-grown undoped GaN surface exposed and a DC potential of 6 V applied to the sample with respect to an inert platinum counter electrode. No SiO_2 or other protective layer was deposited on the GaN surface, and no trenches were etched. The electrochemical porosification thus proceeds vertically from the top surface, but as we have previously shown,[14] the top surface is left unaffected by the etching process, within the accuracy achieved by atomic force microscopy measurements.

To examine how the porosity evolves with etching time, we used a sample consisting of 12 periods of alternating highly doped and undoped GaN, with the top (surface) layer being undoped. Pieces of the sample were etched for time periods of increasing duration and then cleaved and examined in the scanning electron microscope (SEM) using a Nova NanoSEM with the through lens secondary electron detector and an acceleration voltage of 5 kV. After a short etching period (500 s), porosity is only observed in patches of the uppermost doped layer [Fig. 1(a)]. After 1000 s

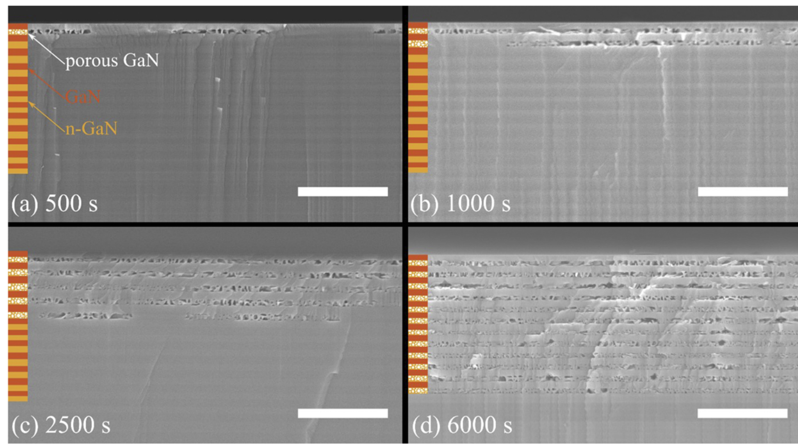

FIG. 1. Cross-sectional SEM images of a DBR sample after various etch times, showing how the etch proceeds in depth as time passes. Scale bars are 1 μm.

© Author(s) 2020

[Fig. 1(b)], porosity is observed throughout the top layer and the second layer has also mostly been porosified. After 2500 s, porosity is observed throughout the top four layers and about half of the fifth is porous [Fig. 1(c)]. In this case, the full 12 pair structure was porosified after 6000 s. The etch proceeds from the top surface down, but the undoped layers between the porous layers remain essentially undamaged within the resolution of the SEM observation. Hence, it is vital to address how the etchant is accessing each doped layer after etching of the previous layer completes and indeed how the etchant accesses the first doped layer through the undoped cap.

In a previous study, we inferred that the etch accesses the sub-surface layers via channels at dislocations,[14] postulating that these defects—usually seen to be a weakness of heteroepitaxial GaN materials—can, in fact, be used to great advantage in engineering the sub-surface porous morphology. Here, we use plan view high angle annular dark field imaging in the scanning transmission electron microscope (HAADF-STEM) to observe the structure of threading dislocation cores in a porous DBR sample and an unetched material from the same wafer (Fig. 2). The HAADF-STEM imaging was performed on an aberration-corrected FEI Titan operated at 300 kV. The sample was prepared in the plan-view geometry by mechanical polishing, followed by Ar^+ ion milling at 5 kV until a hole was visible, and final cleaning at 0.1–1 kV. Dislocations in the sample that has not been porosified exhibit a filled core structure with a range of atomic arrangements, consistent with those previously reported in the literature.[24] Figure 2(a) shows an example of an edge dislocation with the usual core structure consisting of a five-membered and a seven-membered ring. This is in strong contrast with the porosified sample, where the dislocations we observed had a hollow core [Fig. 2(b)]. In Figs. 2(a) and 2(b), a Burgers circuit has been drawn around the suggested position of the dislocation. The Burgers circuit drawn around the ~5–10 nm diameter hole in Fig. 2(b) confirms the existence of an edge- or mixed-type dislocation at the hole location.

Lower magnification HAADF-STEM images of a single porous layer in a porosified sample [Fig. 2(c)] reveal the structure of the porous layer around the holes at the dislocation locations. In Fig. 2(c), the contrast relates to the thickness of the sample (given that all of the material is GaN) and the holes at dislocation locations are seen as dark spots (one of these is ringed in white). Radiating out from these dark spots, we see a finger-like structure, with the pores (dark gray contrast) alternating with bright unetched walls. Domains are observed, which are separated by unetched walls wherever the finger-like pores emanating from different dislocations would otherwise meet. A subset of these walls are marked in yellow in Fig. 2(c). These data suggest that porosification occurs through dislocations, where a dislocation forms a pipe that connects the surface of the sample to a subsurface layer, which is subsequently etched via that pipe.

Very occasionally, we observe domains of pores that have an unetched dislocation core at their center (Fig. 3). However, in this case, we observe a dark region to one side of the dislocation core, indicating that the material is thinner in this region. In this case, we suggest that the pipe connecting the dislocation core to the surface terminates at the porous layer under observation and that the dark recession relates to the pipe position. These rare structures give us the opportunity to assess the strain field around the dislocation and

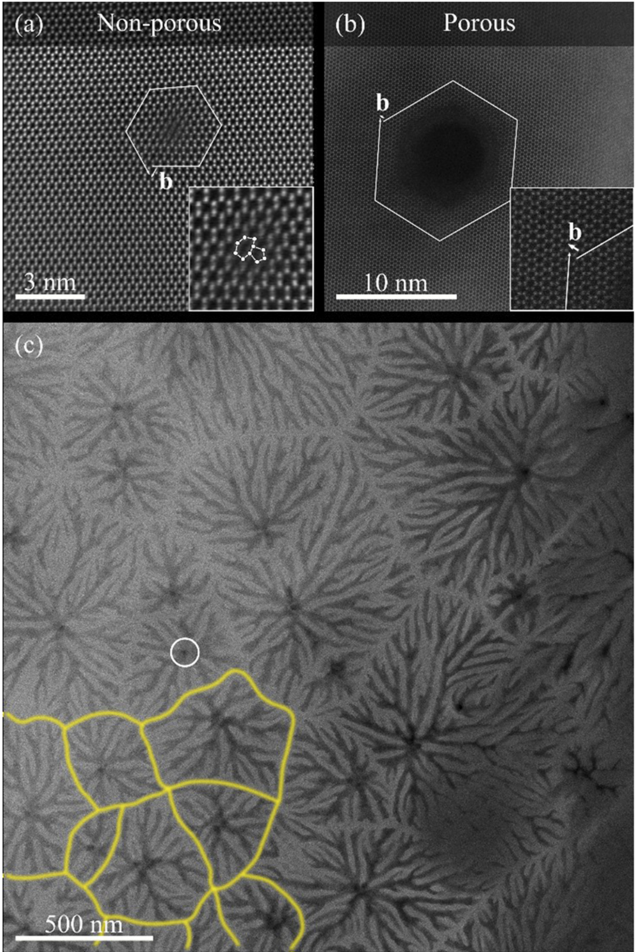

FIG. 2. High resolution HAADF-STEM image of a dislocation seen along the ⟨0001⟩ zone axis (i.e., seen end-on) in the (a) non-porous sample and (b) porous sample. (c) Lower magnification HAADF-STEM image of a porous layer in the porosified sample. Here, contrast is thickness-related (i.e., dark means pore). A hole at the location of a dislocation is marked in white, while a subset of the walls between domains emanating from separate dislocations are marked in yellow.

how it relates to the position of the pipe. The STEM data in Fig. 3 are overlaid with a geometrical phase analysis map,[25] revealing a compressively strained region on one side of the dislocation core and a tensile strained region on the other. The dark region corresponding to the pipe location is located on the same side of the dislocation core as the compressively strained region. Silicon dopants have a tendency to segregate to the compressively strained regions adjacent to dislocation cores.[26] Hence, these observations are consistent with outdiffusion of silicon from the doped to the undoped layers in the vicinity of dislocations. The compressively strained region adjacent to the dislocation core would then have an enhanced conductivity, allowing electrochemical etching to take place. Such silicon segregation would be expected to occur in the very near vicinity of the dislocation core,[26] consistent with our observation of the formation of pipes that remove the core structure. Other unintentional dopant

© Author(s) 2020

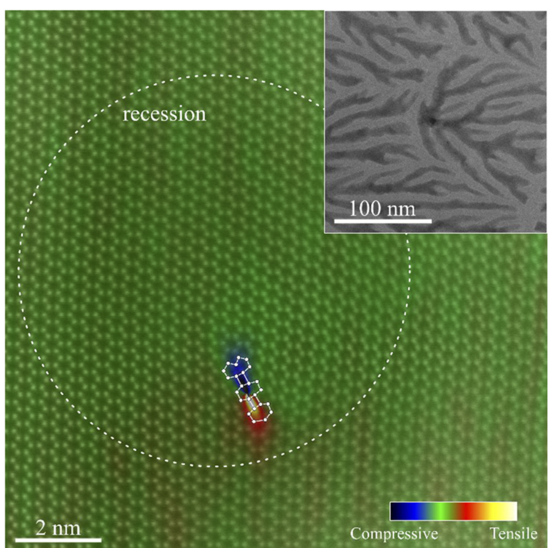

FIG. 3. High resolution HAADF-STEM image of a (dissociated mixed-type) dislocation seen along the ⟨0001⟩ zone axis (i.e., seen end-on) in the porous sample. This dislocation was not etched completely, and a recession from the etch channel could be seen in darker contrast (indicated by a circle). The recession is not centered on the unetched dislocation core but is instead shifted on the compressive region part of the core, as indicated by the geometrical phase analysis overlay. Inset: lower magnification HAADF-STEM image of the same region.

incorporation (e.g., oxygen) could also lead to a conductivity in the near core region, facilitating etching.

It is worth briefly commenting on why the dislocation in Fig. 3 might have an intact core below the etched layer. We suggest that this occurs when etching down different nanopipes occur at slightly different rates, and hence, in the next doped layer below the one pictured in Fig. 3, the material close to this dislocation could have been etched via other, faster etching nanopipes before this etch pathway penetrated below the layer in this figure. Hence, etching down this pathway would terminate, leaving the dislocation core intact.

Based on the TEM data [e.g., Fig. 2(c)], we estimate that the volume fraction of the material removed from the porous layers is approximately 45%. Etch times vary between samples, but the etching of a single layer can take as little as 120 s. Assuming that nitrogen is evolved from the overall etching reaction as N_2 molecules, then for a dislocation density of ca. 3×10^8 cm^{-2} and the formation of pipes at the dislocation core of 5 nm radius, this implies a flux of N_2 down the pipe of roughly 0.03 mol m^{-2} s^{-1}. Assuming that nitrogen is transported via diffusion through the solvent (water) contained in the pipe, we calculate (see the supplementary material) that this rate of mass transport would require a supersaturation of nitrogen in water of around a factor of two in comparison to the equilibrium solubility at atmospheric pressure. Such a super-saturation is not unreasonable, given that the formation of gaseous nitrogen would require the nucleation of gas bubbles, and the critical radius for nucleation might require bubbles to be formed which are larger than the pore size.

Dislocations in GaN are generally considered to be a nuisance, deteriorating the properties of devices. Here, however, we have shown that they can be usefully exploited as pathways for electrochemical etching of sub-surface layers, providing a pipeline for the flow of the etchant through the undoped material and leaving the surrounding defect-free material undamaged. This approach has been shown to be viable not only for the polar GaN studied here but also for non-polar GaN,[14] and our STEM studies (see the supplementary material, Fig. 1) show similar pore morphologies for the non-polar case. Focused ion beam/SEM studies of AlGaN DBRs[23] show a similar morphology to the porous layer, suggesting that the same mechanism operates in other alloys (see the supplementary material, Fig. 2). This flexibility between the different crystal orientations and compositions suggests that defect assisted electrochemical etching may also be viable in other heteroepitaxial semiconductor materials.

See the supplementary material for details of calculations on the rate of mass transport down the pipes at dislocation cores and for images of porous layers formed via dislocation related mechanisms in non-polar GaN and c-plane AlGaN.

This work was supported, in part, by the UK Engineering and Physical Sciences Research Council (EPSRC) under Grant Nos. EP/M011682/1 and EP/M010589/1 and the EPSRC Impact Acceleration Account Follow-On Fund of the University of Cambridge.

DATA AVAILABILITY

The data that support the findings of this study are available within the article and its supplementary material.

REFERENCES

[1] F. A. Ponce and D. P. Bour, Nature **386**, 351 (1997).
[2] S. Kako, C. Santori, K. Hoshino, S. Götzinger, Y. Yamamoto, and Y. Arakawa, Nat. Mater. **5**, 887 (2006).
[3] O. Jani, I. Ferguson, C. Honsberg, and S. Kurtz, Appl. Phys. Lett. **91**, 132117 (2007).
[4] B. J. Baliga, Semicond. Sci. Technol. **28**, 074011 (2013).
[5] F. Tabataba-Vakili, S. Rennesson, B. Damilano, E. Frayssinet, J.-Y. Duboz, F. Semond, I. Roland, B. Paulillo, R. Colombelli, M. E. Kurdi, X. Checoury, S. Sauvage, L. Doyennette, C. Brimont, T. Guillet, B. Gayral, and P. Boucaud, Opt. Express **27**, 11800 (2019).
[6] J.-H. Kang, D. K. Jeong, J.-S. Ha, J. K. Lee, and S.-W. Ryu, Semicond. Sci. Technol. **32**, 025001 (2017).
[7] B. F. Spiridon, P. H. Griffin, J. C. Jarman, Y. Liu, T. Zhu, A. D. Luca, R. A. Oliver, and F. Udrea, Proceedings **2**, 776 (2018).
[8] S.-M. Lee, S.-H. Gong, J.-H. Kang, M. Ebaid, S.-W. Ryu, and Y.-H. Cho, Opt. Express **23**, 11023 (2015).
[9] B. Alshehri, S.-M. Lee, J.-H. Kang, S.-H. Gong, S.-W. Ryu, Y.-H. Cho, and E. Dogheche, Appl. Phys. Lett. **105**, 051906 (2014).
[10] S. Huang, Y. Zhang, B. Leung, G. Yuan, G. Wang, H. Jiang, Y. Fan, Q. Sun, J. Wang, K. Xu, and J. Han, ACS Appl. Mater. Interfaces **5**, 11074 (2013).
[11] L.-W. Jang, D.-W. Jeon, A. Y. Polyakov, A. V. Govorkov, V. N. Sokolov, N. B. Smirnov, H.-S. Cho, J.-H. Yun, K. D. Shcherbatchev, J.-H. Baek, and I.-H. Lee, J. Alloys Compd. **589**, 507 (2014).
[12] D. Cao, H. Xiao, H. Xu, J. Cui, Q. Gao, and H. Pei, Mater. Res. Bull. **70**, 881 (2015).
[13] A. Waseem, D. K. Jeong, M. A. Johar, J.-H. Kang, J.-S. Ha, J. K. Lee, and S.-W. Ryu, Semicond. Sci. Technol. **33**, 065007 (2018).
[14] T. Zhu, Y. Liu, T. Ding, W. Y. Fu, J. Jarman, C. X. Ren, R. V. Kumar, and R. A. Oliver, Sci. Rep. **7**, 45344 (2017).
[15] D. Cao, C. Zhao, X. Yang, and H. Xiao, J. Alloys Compd. **806**, 487 (2019).
[16] S. M. Mishkat-Ul-Masabih, A. A. Aragon, M. Monavarian, T. S. Luk, and D. F. Feezell, Appl. Phys. Express **12**, 036504 (2019).

© Author(s) 2020

[17] K. T. P. Lim, C. Deakin, B. Ding, X. Bai, P. Griffin, T. Zhu, R. A. Oliver, and D. Credgington, APL Mater. **7**, 021107 (2019).
[18] X. Xiao, P. Lu, A. J. Fischer, M. E. Coltrin, G. T. Wang, D. D. Koleske, and J. Y. Tsao, J. Phys. Chem. C **119**, 28194 (2015).
[19] Y. Zhang, S.-W. Ryu, C. Yerino, B. Leung, Q. Sun, Q. Song, H. Cao, and J. Han, Phys. Status Solidi B **247**, 1713 (2010).
[20] S. Mishkat-Ul-Masabih, T. S. Luk, A. Rishinaramangalam, M. Monavarian, M. Nami, and D. Feezell, Appl. Phys. Lett. **112**, 041109 (2018).
[21] K.-P. Huang, K.-C. Wu, F.-H. Fan, W.-P. Tseng, B.-C. Shieh, S.-H. Chen, and C.-F. Lin, ECS J. Solid State Sci. Technol. **3**, R185 (2014).
[22] W.-J. Hsu, K.-T. Chen, W.-C. Huang, C.-J. Wu, J.-J. Dai, S.-H. Chen, and C.-F. Lin, Opt. Express **24**, 11601 (2016).
[23] P. Griffin, T. Zhu, and R. Oliver, Materials **11**, 1487 (2018).
[24] S. K. Rhode, M. K. Horton, M. J. Kappers, S. Zhang, C. J. Humphreys, R. O. Dusane, S.-L. Sahonta, and M. A. Moram, Phys. Rev. Lett. **111**, 025502 (2013).
[25] M. J. Hÿtch, E. Snoeck, and R. Kilaas, Ultramicroscopy **74**, 131 (1998).
[26] S. L. Rhode, M. K. Horton, W. Y. Fu, S.-L. Sahonta, M. J. Kappers, T. J. Pennycook, C. J. Humphreys, R. O. Dusane, and M. A. Moram, Appl. Phys. Lett. **107**, 243104 (2015).

© Author(s) 2020